American Mineralogist, Volume 78, pages 877–883, 1993

Tunneling spectroscopy applied to PbS (001) surfaces: Fresh surfaces, oxidation, and sorption of aqueous Au

CARRICK M. EGGLESTON*
Department of Applied Earth Sciences, Stanford University, Stanford, California 94305-2225, U.S.A.
MICHAEL F. HOCHELLA, JR.**
Department of Geology, Stanford University, Stanford, California 94305-2115, U.S.A.

ABSTRACT

Electron tunneling spectroscopy (ETS) makes possible the study of electronic structures of conductive mineral surfaces and can be applied under ambient or in-situ conditions rather than in a vacuum. We use ETS to study fresh, oxidized, and aqueous-Au-treated PbS (001) surfaces in order to demonstrate the strengths and limitations of the technique in the context of a geochemical application. Experimental tunneling spectra are in qualitative agreement with tunneling theory. Spectra for Au, fresh PbS, and oxidized PbS are different (primarily because of work function differences) and can be used to distinguish between, for example, Au and PbS when they are present on one surface. ETS is thus useful as a compositional probe with high spatial resolution. Spectra for fresh PbS show a small peak at about +250 mV that corresponds to conduction band states with mixed Pb and S character. Both the ETS spectra and STM images suggest that these states are lost upon oxidation. Au precipitated on PbS from aqueous $AuCl_4^-$ solutions as isolated islands looks identical to metallic Au in ETS.

INTRODUCTION

For natural Earth surface systems, it may be argued that virtually all chemical processes are modulated or controlled by reactions involving mineral surfaces (Stumm, 1992). Understanding mechanisms of mineral surface reactions depends on a knowledge of surface electronic structures because, fundamentally, interactions between a solid surface and gases, H_2O, or aqueous solutes are interactions between the electronic structures of the adsorbates and of the surface.

Surface electronic structure is commonly studied by photoelectron spectroscopy (PES). X-ray PES (XPS) is often used to study surface compositions (e.g., surface leaching during dissolution) using relative intensities of core-level photoelectron peaks (e.g., Berner and Holdren, 1979; Hellmann et al., 1990). XPS peaks may also have structure that can be related to specific surface species (e.g., Stipp and Hochella, 1991). UV-PES (UPS) is used to examine valence-band electronic structures related to bonding. The valence band is also accessible to electron tunneling spectroscopy (ETS). Some forms of ETS have been in use for several decades, but the technique described here is based on scanning tunneling microscopy (STM), which, along with scanning force microscopy (SFM), is being used in geosciences primarily for imaging of microtopography and surface atomic and molecular structure. Here, we apply ETS to PbS (galena) surfaces and to changes in surface electronic structure associated with oxidation and sorption of aqueous Au. This system was chosen because it is an experimentally convenient analogue for natural systems for Au scavenging and concentration.

PREVIOUS WORK

ETS has been used in many vacuum-based studies of metal and semiconductor surfaces; Stroscio et al. (1986), Feenstra et al. (1987a, 1987b), and Avouris (1990) provided good examples. For minerals, Gilbert and Kennedy (1989) studied tunneling hysteresis on Fe_2O_3 and TiO_2 surfaces using ambient ETS, and Sakamaki et al. (1990) applied ambient ETS to TiO_2 to study surface density of states (DOS). Fan and Bard (1991) studied pyrite {100} surface DOS; their results are in agreement with those of Eggleston and Hochella (1992) based on UPS and STM. Eggleston and Hochella (1991) used ETS to distinguish between Au and PbS on PbS {100} surfaces that had been exposed to aqueous gold chloride; this paper presents the basis of, and an expansion upon, these earlier results.

THEORY

Electron tunneling theory, as applied to STM and ETS, is well summarized in Stroscio et al. (1986), Feenstra et al. (1987a), Avouris (1990), and references therein. For a tip-surface tunneling junction, the tunneling current (I_T)

* Present address: Institute for Water Resources and Water Pollution Control, Swiss Federal Institutes of Technology, CH-8600 Dübendorf, Switzerland.
** Present address: Department of Geological Sciences, Virginia Polytechnic Institute and State University, Blacksburg, Virginia 24061, U.S.A.

0003–004X/93/0910–0877$02.00

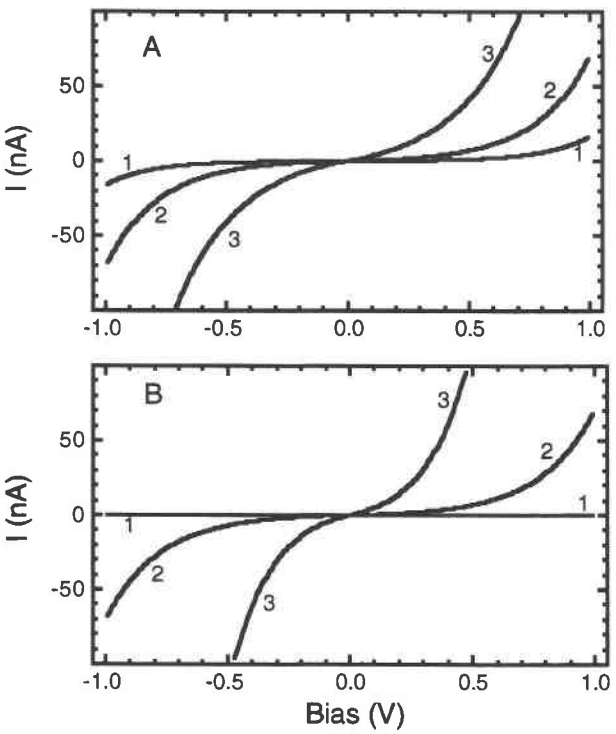

Fig. 1. Calculated I_T vs. V_b curves for (**A**) varying tip-sample separation, s: (1) 12, (2) 10, and (3) 8 Å, with $\Phi = 1$ eV in all cases; and for (**B**) various barrier heights, Φ: (1) 2, (2) 1, and (3) 0.6 eV, with $s = 10$ Å in all cases.

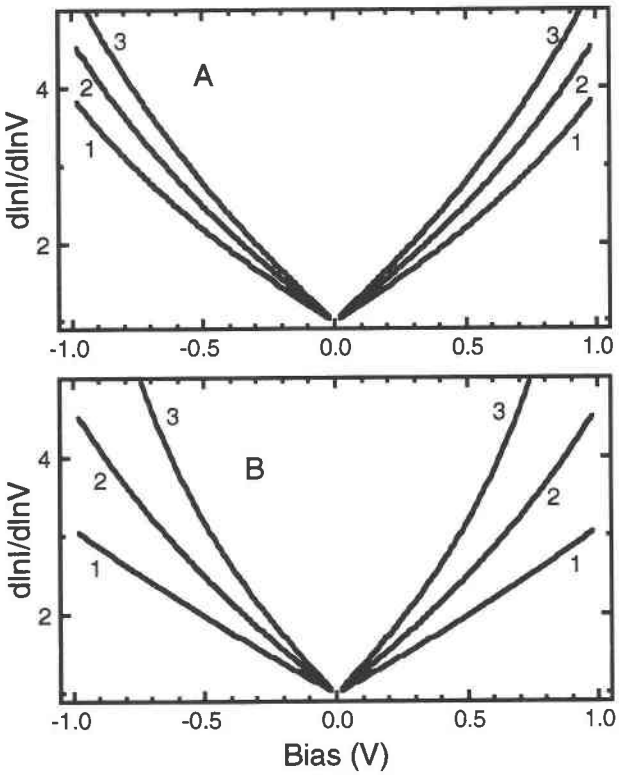

Fig. 2. Calculated (d ln I_T)/(d ln V_b) curves corresponding to I_T vs. V_b curves of Fig. 1, for (**A**) varying tip-sample separation, s: (1) 12, (2) 10, and (3) 8 Å, with $\Phi = 1$ eV in all cases; and for (**B**) various barrier heights: (1) 2, (2) 1, and (3) 0.6 eV, with $s = 10$ Å in all cases.

can be written

$$I_T = \int_{E_F}^{E_F + eV_b} \rho_S(E, \mathbf{r})\rho_T(E_F - eV_b, \mathbf{r}) \exp\left[-s\sqrt{(2m/\hbar^2)(\Phi - eV_b/2)}\right] dE \quad (1)$$

where V_b is the bias voltage across the junction, E_F is the Fermi level, ρ_S and ρ_T are sample and tip density of (electron) states (DOS) functions at the location of the tip $\mathbf{r}$ and energy $E = eV_b$, Φ is the barrier height [$\Phi = (\phi_S + \phi_T)/2$, where ϕ_T and ϕ_S are the work functions of tip and sample, respectively], m is the electron rest mass, $\hbar$ is Planck's constant divided by 2π, and s is the tip-sample separation distance. The exponential term expresses the conductance of the junction.

Differentiation of Equation 1 and normalization to Ohm's Law conductance (I/V) gives a function [$(dI_T/dV_b)/(I/V)$] proportional to the convolved DOS of the tip and sample (Stroscio et al., 1986) in the limit of low V_b. A plot of $(dI_T/dV_b)/(I/V)$ or the mathematically equivalent function (d ln I_T)/(d ln V_b) vs. V_b should give peaks at energies corresponding to high DOS. However, because the conductance of the tunnel junction does not follow Ohm's Law but is a function of V_b, DOS information is superimposed on a smoothly varying background whose characteristics depend on Φ and s.

To show the dependence of the background on Φ and s, we calculated I_T vs. V_b and (d ln I_T)/(d ln V_b) vs. V_b curves for various s and Φ values using the equation $I_T = AV_b\exp(-sB\sqrt{\Phi - eV_b/2})$, a simplified version of Equation 1 used by Binnig et al. (1982) and Binnig and Rohrer (1986) in describing their original STM and ETS work. The constant A ($A = 10^{-4}$/Ohm in our case) was chosen to give realistic currents for a given V_b, and $B = (2m/\hbar^2)^{1/2}/2 = 1.025\ eV^{-1/2}$/Å.

Figure 1 shows calculated I_T vs. V_b curves, and Figure 2 shows the corresponding (d ln I_T)/(d ln V_b) vs. V_b curves. Figure 1A shows I_T vs. V_b curves for different tip-sample separations, s; I_T is very sensitive to s, as expected from theory. The corresponding (d ln I_T)/(d ln V_b) curves (Fig. 2A) are not very sensitive to s, however, unless s varies by $> \pm 2$ Å. Figure 1B shows I_T vs. V_b for different barrier heights; Figure 2B shows that the slope of (d ln I_T)/(d ln V_b) vs. V_b is very sensitive to factor of two changes in Φ.

Figures 1 and 2 thus show the form of the smoothly varying background in the absence of varying DOS structure. For samples exhibiting DOS structure, peaks in (d ln I_T)/(d ln V_b) or $(dI_T/dV_b)/(I_T/V_b)$ spectra are found to correspond to bands of high DOS; excellent examples of this for UHV conditions may be found in Stroscio et al. (1986) and Avouris (1990).

Because our STM and ETS were performed in ambient conditions, we must consider differences between ambient and vacuum tunneling. First, under ambient conditions, the tip-sample gap contains positive charge (the intervening atomic nuclei) that may alter the shape and height of the tunneling barrier Φ (Simmons, 1963). Generally, Φ is lower under ambient conditions that in UHV. Second, chemisorbates alter the surface electronic structure.

These problems present serious complications for ambient ETS, but do not preclude its usefulness in well-defined applications. In practice, only resonant processes (those whose frequency or time scale is similar to that of data measurement) are likely to hamper data collection seriously. For example, if the tip is slightly oxidized, the tip-sample gap contains an oxide layer, but the dielectric properties of the oxide may be treated as constant unless the oxide layer grows during use of the tip. A more serious problem is that adsorbates surface diffuse and may exchange onto and off of surface sites at high frequency. A variety of sorbate-induced electronic structures may occur and recur locally; peaks from particular structures are likely to be averaged out, leaving only a featureless background. However, if a particular structure dominates the time average and the tip is also temporally stable, specific peaks may be observed. The fact that STM imaging is possible under ambient conditions supports this conclusion; when imaging is successful, we are probing states that should also be spectroscopically observable.

Experimental

STM and ETS were performed using a Digital Instruments Nanoscope II. W tips were made by electrochemical etching in 1 *M* solution of KOH. Instrument conditions are reported in the figure captions. Tunneling spectra were obtained using a cycle in which the feedback loop ran for 300 μs at a given V_b and setpoint I_T (I_{set}) to stabilize the tip-sample separation, then an I_T vs. V_b or (d ln I_T)/(d ln V_b) spectrum was obtained; the cycle was repeated a specified number of times (see figure captions) for signal-averaged spectra. Stabilization of s was necessary to avoid tip crashes (contact between tip and sample, giving Ohmic conduction and changes in tip properties).

The (d ln I_T)/(d ln V_b) spectra were obtained by modulating V_b at each increment of V_b and calculating Δ(ln I_T)/Δ(ln V_b) from ln I_T and ln V_b at the high and low ends of the V_b modulation. The V_b modulation was 20–30 mV, much smaller than the total V_b range sampled in the spectrum. At very low V_b (i.e., where V_b is less than the V_b modulation and where noise in I_T dominates the I_T being measured or is large compared with it), the calculation of Δ(ln I_T)/Δ (ln V_b) often blows up, giving spikes in the data near E_F. Such artifacts are obvious in our data. Our amplifier saturated at 50 nA; most of our spectra were obtained within a voltage range of -1 and $+1$ V but nevertheless saturate the amplifier, causing dI_T/dV_b and therefore (d ln I_T)/(d ln V_b) to go to zero. In single spectra this cutoff is abrupt, but for averaged spectra, because the cutoff V_b varies in each spectrum, the cutoff appears gradual. High I_T values cause the V_b applied to the sample to be less than the V_b desired by an amount that depends on I_T (an Ohmic effect of the I_T measurement system, approximately 1 mV/nA). The effects are sufficiently small so that no important consequences were observed.

STM images and ETS spectra were obtained for several materials, all at room temperature. Au films were grown on cleaved muscovite at 10^{-7} torr and 500 °C (see Lang et al., 1989). PbS crystals were cleaved under polyphenyl ether, a nonpolar oil (in order to exclude air; see Eggleston and Hochella, 1990 or 1991); these surfaces give relatively stable images and spectra. PbS surfaces that had been in H_2O for 1 min or in air for five months were also examined under oil in order to maintain comparability of the tunneling medium and to prevent further reaction with air. XPS studies of PbS oxidation (e.g., Buckley and Woods, 1984) show that after five months of air exposure PbS surfaces exhibit evidence of Pb-O bonding and sulfate-like species; we designate this surface "oxidized PbS." Finally, fresh PbS surfaces were exposed to 1.3 ppm $KAuCl_4$, 1.1 *M* NaCl solution at pH = 3.2 (adjusted with HCl) at room temperature for periods from 1 min to 60 h.

Results and discussion

Figure 3 shows I_T vs. V_b spectra for (A) Au foil, (B) fresh PbS, and (C) oxidized PbS, at several tip-sample separations, s, in each case; the exact value of s is unknown, but the s variation is probably <2 or 3 Å. The data in Figure 3 are labeled with the feedback I_{set} (in units of nanoamps), which fixes s; the higher I_{set}, the lower s. The data are nonlinear with increasing V_b, as expected for tunneling conduction (Fig. 1).

The spectra for different materials have different shapes; note, for example, the curves marked 1 nA in each case. The spectra for Au foil are easily distinguished from those for both fresh and oxidized PbS, and at least the 1-nA curves are distinct for fresh and oxidized PbS. Because the feedback loop ran at +200 mV and at the I_{set} marked on each curve, the data in Figure 3 should intersect these I_{set} values at +200 mV. That is not always the case, probably because of drift in s during data measurement. Figure 3C shows variability in I_T vs. V_b curves for a sequence of ten spectra (labeled 1 nA). Uncertainties were a small fraction of 1 nA at low V_b and ± 8 nA at high V_b.

The differences among the I_T vs. V_b spectra for the different materials were also apparent in the (d ln I_T)/(d ln V_b) data (Fig. 4). The more curved the I_T vs. V_b spectrum in Figure 3 (i.e., the greater d^2I_T/dV_b^2), the steeper the (d ln I_T)/(d ln V_b) function in Figure 4, as expected (e.g., see Figs. 1B and 2B). For example, dI_T/dV_b for the data for Au foil in Figure 3A is nearly constant, so (dI_T/dV_b)/(I/V) should also be nearly constant, as in Figure 4A. The data in Figures 3 and 4 suggest that ETS may be used as a high spatial-resolution compositional identification or differentiation tool, at least for compositionally constrained systems. The reasons for the differences in

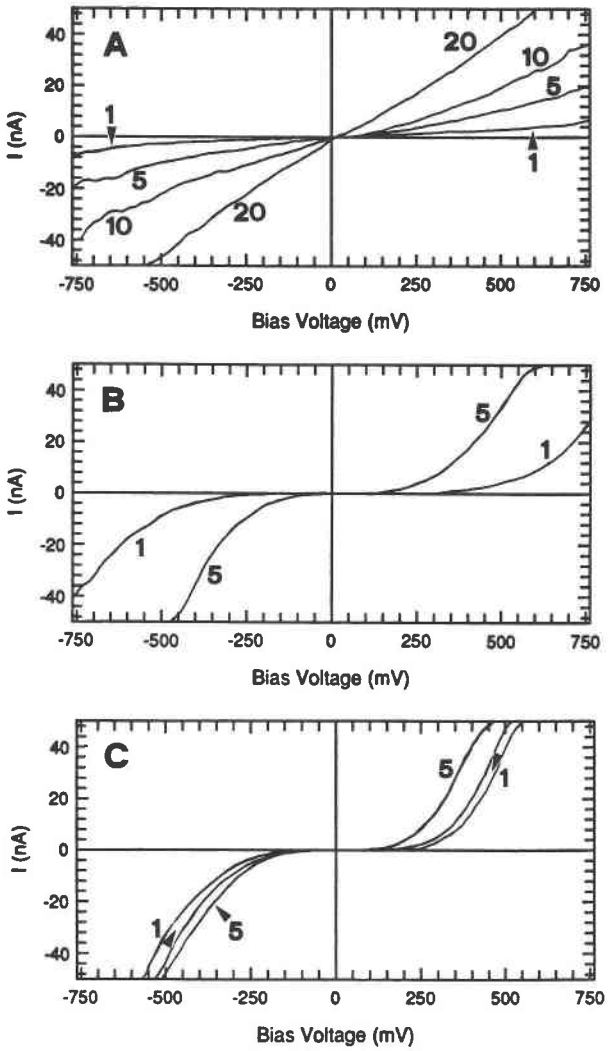

Fig. 3. I_T vs. V_b curves for (**A**) Au foil, (**B**) freshly cleaved PbS, and (**C**) oxidized PbS. Each curve is labeled with the feedback I_{set} in nanoamps (at +200 mV), which determines the tip-sample distance. The higher I_{set} is, the closer the tip is to the sample. Each curve is the average of five individual scans. In **C**, the pair of curves joined by the bases of the arrows show the range of curves obtained in ten successive spectra.

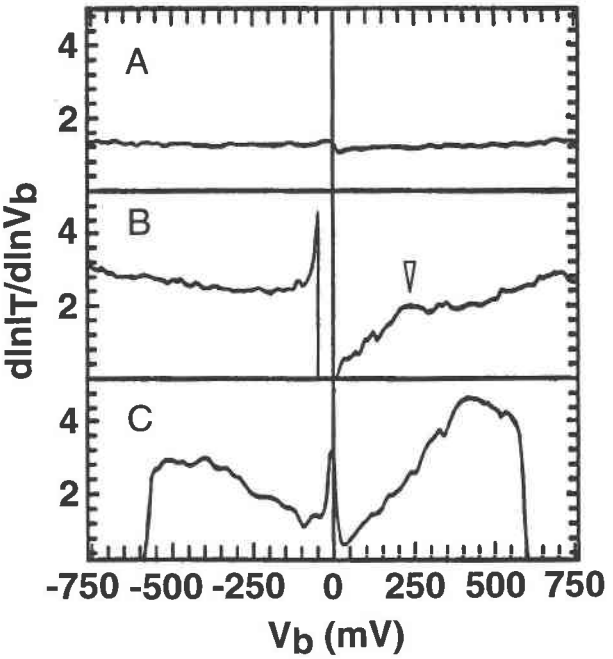

Fig. 4. Signal-averaged (d ln I_T)/(d ln V_b) spectra for (**A**) Au foil, (**B**) freshly cleaved PbS, and (**C**) oxidized PbS. The feedback loop was running at +200 mV and 1 nA between the ten data measurement cycles for all spectra. **B** shows a faint but reproducible peak for fresh PbS at about +250 mV (arrow). The general shape of **C** was reproducible, but details of the spectra were not (compare with Figs. 6C, 7C, and 7D).

the spectra in Figures 3 and 4 requires explanation if the general applicability of ETS is to be extended.

As discussed above, variation in the slope of (d ln I_T)/(d ln V_b) spectra may arise from (1) differences in tip-sample separation, s, (2) different barrier heights, and (3) DOS variations. We collected spectra for Au and oxidized PbS for different tip-sample separations and found little dependence of the slope of the (d ln I_T)/(d ln V_b) curves on s, in agreement with Figure 2A. The work function of Au metal (ϕ_{Au}) is about 5.2 eV (Zangwill, 1988), and the work function of PbS (ϕ_{PbS}) is about 3.7 eV (Evans and Raftery, 1982). The work function of oxidized PbS is not well defined but is almost certainly less than for fresh surfaces. According to the calculations (Fig. 2B), these differences should cause the slope of the (d ln I_T)/(d ln V_b) vs. V_b curves to be arranged in the order $PbS_{oxidized} > PbS_{fresh} > Au$, in agreement with observation (Fig. 4). Therefore, the different slopes are probably due at least partly, and perhaps mostly, to work function differences among the materials.

The data in Figure 4 seem consistent with the expectation for the DOS of a metal relative to a semiconductor; a metal should have a relatively even DOS across E_F, whereas a semiconductor such as PbS, with a surface band gap of 0.1–0.4 eV, should show increasing DOS away from E_F. However, if the DOS were the only contribution, the (d ln I_T)/(d ln V_b) function should have a more abrupt increase in slope as eV_b exits the band gap and valence or conduction band states begin to contribute to the tunneling current. Figure 4, with the exception of Figure 4B, instead shows a steady increase in (d ln I_T)/(d ln V_b) with V_b, a form more consistent with the form of curves in the absence of DOS structure (e.g., see Fig. 2). The exception, Figure 4B, is discussed below in regard to PbS oxidation.

PbS OXIDATION

Figure 4B shows a broad peak in the (d ln I_T)/(d ln V_b) function at about +250 mV. Although we did not expect DOS peaks to be observable in ambient (rather than vacuum) conditions, the reproducibility of this peak (in sev-

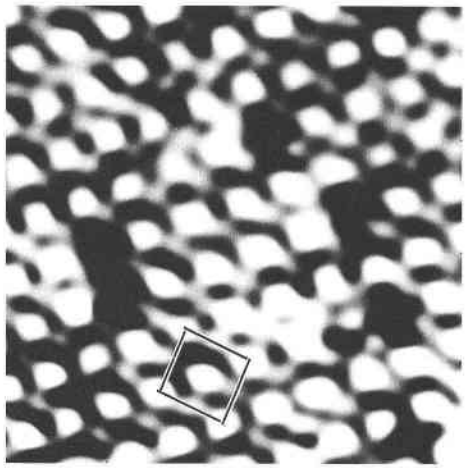

Fig. 5. STM image of a PbS surface taken after a 1-min exposure to deionized H_2O, at +200 mV and 1 nA in the constant height mode. Contrast is due to variation in I_T. This image was taken only a few nanometers from the area imaged in Eggleston and Hochella (1991). According to the interpretation of Eggleston and Hochella (1990), the bright sites correspond to S and the less bright sites correspond to Pb. A unit cell with corners on S sites is marked. The measured edge length is 6 ± 0.2 Å, within error of the expected unit-cell edge length of 5.97 Å. The fresh galena surface structure is seen in most of the image (compare with Eggleston and Hochella, 1990); in addition, five apparent vacancies (probably oxidized sites) are evident. The image is low-pass filtered (cutoff = 0.4 Å) to remove high-frequency noise. Drift causes slight distortion of the nominally square unit cell.

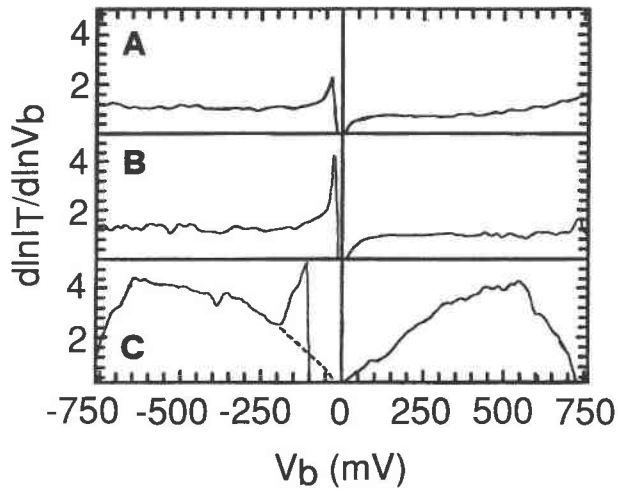

Fig. 6. Signal-averaged (ten cycles) (d ln I_T)/(d ln V_b) spectra for (**A**) Au precipitated on PbS after 60 h of exposure to the Au solution (see text), (**B**) an Au island grown on PbS after a 1.5-h exposure to the Au solution, and (**C**) oxidized PbS between Au islands on the same sample as in **B**. V_b and I_{set} were +200 mV and 1 nA, respectively. The dotted line in **C** shows the region of the spectrum obscured by the blow-up of the (d ln I_T)/(d ln V_b) calculation (see experimental section).

eral hundred successive spectra) suggests that it is real. Figure 5 is an STM image taken at similar V_b (+200 mV). We interpret the peak in Figure 4B as the spectroscopic expression of the same band of states imaged in Figure 5 (excluding the apparent vacancies), i.e., a band of conduction-band states with mixed Pb and S character.

The DOS spectra for oxidized PbS do not show a discernible peak at +250 mV and were quite variable. Eggleston and Hochella (1991) showed that the apparent vacancies in images similar to Figure 5 probably correspond to oxidized S sites. These sites are probably not vacant but rather are sites of reduced I_T resulting from shifts in electronic structure related to oxidation. It seems reasonable to suggest that we do not observe the +250 mV DOS peaks in (d ln I_T)/(d ln V_b) spectra of oxidized PbS for the same reason that we see vacancies in the STM images of incipiently oxidized PbS surfaces; i.e., oxidation of surface S sites reduces the local DOS at this energy. It can be argued that we are observing, on the atomic scale, the beginnings of the process by which Pb-O and S-O bonding widens the band gap by removing state density near E_F. However, it must be remembered that ETS spectra and STM images depend on stable tip configurations and other variables, and our inability to observe an ETS peak on oxidized surfaces may merely reflect unstable tips or the averaging out of peaks from a variety of individually short-lived structures. The important result is that the PbS conduction band states within 200–250 mV of E_F can be observed in both ETS and STM under ambient conditions, given stable tip, tunneling medium, and drift conditions.

Sorbed Au

Reductive sorption of aqueous Au complexes to sulfides is thought to be important in the formation of certain Au deposits (Seward, 1973; Hyland and Bancroft, 1989; Bakken et al., 1989). The Au-PbS system is ideal for the application of ETS and STM because both the substrate and adsorbate are conductive. Eggleston and Hochella (1991) used ETS to distinguish between Au and PbS on surfaces containing both materials; here, we give further examples of ETS application to the Au-PbS system and compare it with similar systems studied in UHV.

Figure 6A shows a (d ln I_T)/(d ln V_b) spectrum for a PbS surface that had been exposed to the Au (III) chloride solution (see experimental section) for 60 h. The surface was completely covered by Au after this treatment and appeared visibly gilded. The Au precipitated on the PbS surface is spectroscopically indistinguishable from the Au foil (see Fig. 4A). Figure 6B shows a (d ln I_T)/(d ln V_b) spectrum take atop an island grown on a PbS surface after 1.5 h of exposure to the Au solution (STM images in Eggleston and Hochella, 1991, show that the Au exists on the surface as discrete islands up to 1000 Å in length). The spectrum appears identical to that of Au foil and of Au on PbS after longer exposure times. In contrast, Figure 6C shows a (d ln I_T)/(d ln V_b) spectrum taken on the same sample as in Figure 6B, but on an area between the

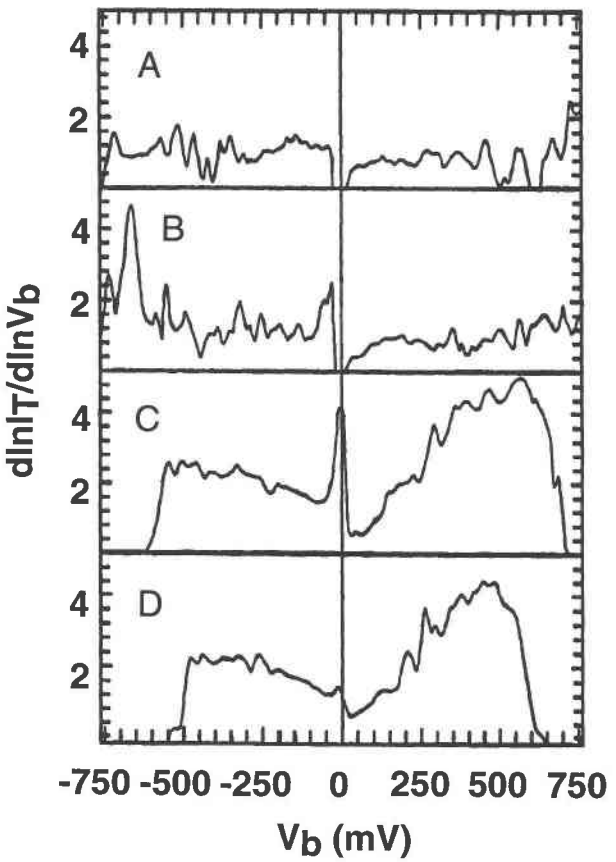

Fig. 7. Sequence of individual (nonaveraged) (d ln I_T)/(d ln V_b) spectra taken with the tip originally positioned over an Au island on a PbS surface. As the Au island drifted out from underneath the tip, spectra characteristic of Au (**A** and **B**) were replaced by spectra characteristic of oxidized PbS (**C** and **D**).

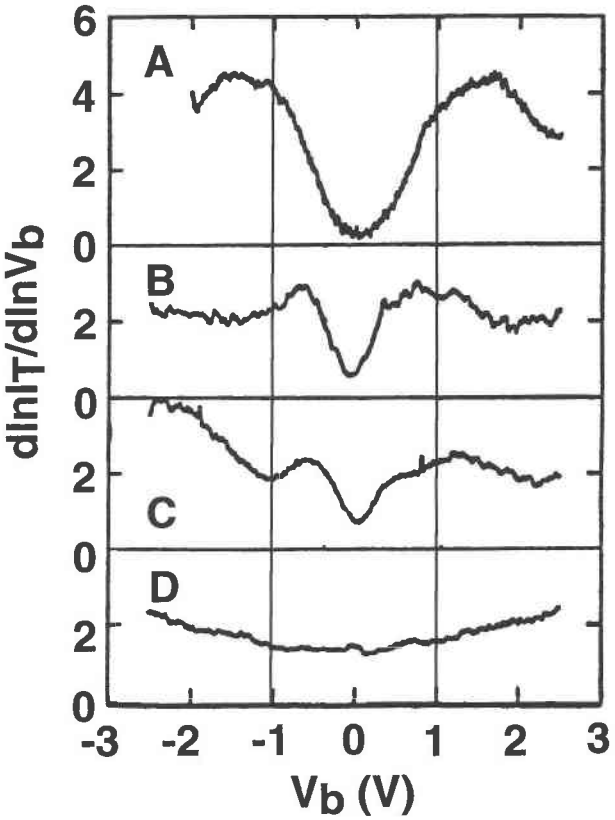

Fig. 8. Spatially averaged DOS spectra from Feenstra (1989) for various coverages of Au on p-GaAs surfaces taken in UHV: (**A**) 1, (**B**) 2, (**C**) 3, and (**D**) 5 ML. The data are similar to our results for Au on PbS, particularly in the range sampled in our study, −750 to +750 mV.

islands; in this case, the spectrum appears similar to those for oxidized galena (see Fig. 4C).

Another example is given in Figure 7. The tip was positioned over an Au island and a sequence of spectra collected. Although the spectra are quite noisy, the first two (Fig. 7A, 7B) are typical of Au. During several minutes the tip was allowed to drift, and when the tip had drifted entirely off of the Au island, oxidized PbS-type spectra were obtained (Fig. 7C, 7D).

Despite the difficulties of ambient ETS, our results are remarkably similar to those for comparable systems studied in UHV. The use of ETS to identify small Au islands on a semiconductor (Si) surface on the basis of work function differences was the first spectroscopic application of STM (Binnig et al., 1982; Binnig and Rohrer, 1987). Another comparable study is summarized in Figure 8, which shows spatially averaged ETS spectra for different coverages of Au on a GaAs(110) surface in UHV (Feenstra, 1989). Because Au forms clusters on the GaAs(110) surface, the data for what is ideally called one monolayer coverage (ML) consist of average spectra for both Au and GaAs (although the author suggests that this is not the case, his STM images show some GaAs between the Au clusters, and, given that what is imageable is also observable spectroscopically, the spectra should contain a contribution from GaAs). At higher coverages (e.g., 5 ML), the GaAs is completely covered by Au. Although Feenstra's data cover a wider voltage range than ours, his spectra are very similar to ours for Au on PbS in the range sample in our study, −750 to +750 mV; the spectrum for Au is flat, whereas that for GaAs rises away from E_F. This is a clear demonstration that differences between Au metal and a semiconductor, particularly work function differences (expressed in the tunneling barrier), are apparent in both UHV and ambient conditions.

Concluding remarks

STM images of topographically complicated surfaces often contain little clue as to the compositional identity of features in the images. We have demonstrated that ETS can be used to identify such features in STM images, if the compositional possibilities are limited. The ETS differences among materials in this study are probably mostly due to work function differences. With stable tips,

we observed a DOS peak in ETS spectra taken in ambient conditions of a fresh PbS surface; the peak corresponds to PbS conduction band states. Spectra of Au precipitated on PbS from aqueous Au(III) solutions confirm that the Au is metallic. This has been demonstrated using XPS (e.g., Hyland and Bancroft, 1989), but it shows that ETS is applicable as an in-situ or ambient-conditions probe with ultrahigh spatial resolution that can, in some cases, be used instead of a UHV technique.

With the minimization of drift and maximization of data collection speed, chemical characterization of conducting or semiconducting mineral surfaces may also be performed in situ and ultimately with near-atomic resolution. ETS is thus a promising tool for the study of surface electronic structure under ambient (rather than UHV) conditions, with applications in mineralogical and geochemical research.

Acknowledgments

We thank B. Bakken, G. Parks, G. Brown, Jr., J. Peck, C. Lang, and S. Stipp for helpful discussions, assistance, or materials. C.M.E. dedicates this paper and ongoing efforts to the late Noye M. Johnson. The Center for Materials Research at Stanford University provided financial and instrumental support. This work was also supported by the Petroleum Research Fund (administered by the American Chemical Society) and the National Science Foundation (grants PRF-22892-AC5,2 and EAR-91-05000, respectively, both to M.F.H.).

References cited

Avouris, P. (1990) Atom-resolved surface chemistry using the scanning tunneling microscope. Journal of Physical Chemistry, 94, 2246–2256.

Bakken, B.M., Hochella, M.F., Jr., Marshall, A.F., and Turner, A.M. (1989) High resolution microscopy of gold in unoxidized ore from the Carlin mine, Nevada. Economic Geology, 84, 171–179.

Berner, R.A., and Holdren, G.R., Jr. (1979) Mechanism of feldspar weathering. II. Observations of feldspars from soils. Geochimica et Cosmochimica Acta, 43, 1173–1186.

Binnig, G., and Rohrer, H. (1986) Scanning tunneling microscopy. IBM Journal of Research and Development, 30, 355–369.

——— (1987) Scanning tunneling microscopy: From birth to adolescence. Reviews of Modern Physics, 59, 615–625.

Binnig, G., Rohrer, H., Gerber, Ch., and Weibel, E. (1982) Surface studies by scanning tunneling microscopy. Physical Review Letters, 17, 57–61.

Buckley, A.N., and Woods, R. (1984) An X-ray photoelectron spectroscopic study of the oxidation of galena. Applications of Surface Science, 17, 401–414.

Eggleston, C.M., and Hochella, M.F., Jr. (1990) Scanning tunneling microscopy of sulfide surfaces. Geochimica et Cosmochimica Acta, 54, 1511–1517.

——— (1991) Scanning tunneling microscopy of galena (100) surface oxidation and sorption of aqueous gold. Science, 254, 983–986.

——— (1992) Scanning tunneling microscopy of pyrite {100}: Surface structure and step reconstruction. American Mineralogist, 77, 221–224.

Evans, S., and Raftery, E. (1982) Electron spectroscopic studies of galena and its oxidation by microwave-generated oxygen species and by air. Journal of the Chemical Society, Faraday Transactions, 78, 3545–3560.

Fan, F.-R., and Bard, A.J. (1991) Scanning tunneling microscopy and tunneling spectroscopy of *n*-type iron pyrite (*n*-FeS_2) single crystals. Journal of Physical Chemistry, 95, 1969–1976.

Feenstra, R.M. (1989) Scanning tunneling microscopy and spectroscopy of gold on the GaAs(110) surface. Journal of Vacuum Science and Technology, B7, 925–930.

Feenstra, R.M., Stroscio, J.A., and Fein, A.P. (1987a) Tunneling spectroscopy of the Si(111)2×1 surface. Surface Science, 181, 295–306.

Feenstra, R.M., Stroscio, J.A., Tersoff, J., and Fein, A.P. (1987b) Atom-selective imaging of the GaAs(110) surface. Physical Review Letters, 58, 1192–1195.

Gilbert, S.E., and Kennedy, J.H. (1989) Observation of hysteresis induced by the tip field in scanning tunneling microscope spectroscopic probing of TiO_2 and α-Fe_2O_3 single-crystal surfaces. Langmuir, 5, 1412–1415.

Hellmann, R., Eggleston, C.M., Hochella, M.F., Jr., and Crerar, D.A. (1990) The formation of leached layers on albite surfaces during dissolution under hydrothermal conditions. Geochimica et Cosmochimica Acta, 54, 1267–1281.

Hyland, M.M., and Bancroft, G.M. (1989) An XPS study of gold deposition at low temperature on sulphide minerals: Reducing agents. Geochimica et Cosmochimica Acta, 53, 367–372.

Lang, C.A., Dovek, M.M., Nogami, J., and Quate, C.F. (1989) Au(111) autoepitaxy studied by scanning tunneling microscopy. Surface Science, 224, L947–L955.

Sakamaki, E., Itoh, K., Fujishima, A., and Gohshi, Y. (1990) Surface density of states of TiO_2 (110) single crystal and adsorbed molecular observation by scanning tunneling microscopy and tunneling spectroscopy. Journal of Vacuum Science and Technology, A8, 614–617.

Seward, T.M. (1973) Thio complexes and the transport of gold in hydrothermal ore solutions. Geochimica et Cosmochimica Acta, 37, 379–399.

Simmons, J.G. (1963) Generalized formula for the electric tunnel effect between similar electrodes separated by a thin insulating film. Journal of Applied Physics, 34, 1793–1803.

Stipp, S.L., and Hochella, M.F., Jr. (1991) Structure and bonding environments at the calcite surface as observed with X-ray photoelectron spectroscopy (XPS) and low energy electron diffraction (LEED). Geochimica et Cosmochimica Acta, 55, 1723–1736.

Stroscio, J.A., Feenstra, R.M., and Fein, A.P. (1986) Electronic structure of the Si(111)2×1 surface by scanning tunneling microscopy. Physical Review Letters, 57, 2579–2582.

Stumm, W. (1992) Chemistry of the solid-water interface, 430 p. Wiley, New York.

Zangwill, A. (1988) Physics at surfaces, 454 p. Cambridge University Press, Cambridge, U.K.

Manuscript received June 26, 1992
Manuscript accepted April 25, 1993